

## Precision measurement of the $^{210}\text{Bi}$ $\beta$ spectrum

I. E. Alekseev <sup>1</sup>, S. V. Bakhlanov,<sup>2</sup> A. V. Derbin <sup>2</sup>, I. S. Drachnev <sup>2</sup>, I. M. Kotina,<sup>2</sup> I. S. Lomskaya <sup>2</sup>, V. N. Muratova,<sup>2</sup>  
N. V. Niyazova,<sup>2</sup> D. A. Semenov,<sup>2</sup> M. V. Trushin,<sup>2</sup> and E. V. Unzhakov<sup>2</sup>

<sup>1</sup>*V.G. Khlopin Radium Institute, St. Petersburg 194021, Russia*

<sup>2</sup>*Petersburg Nuclear Physics Institute, National Research Center “Kurchatov Institute”, Gatchina 188350, Russia*

 (Received 5 June 2020; revised 28 August 2020; accepted 14 December 2020; published 31 December 2020)

The precision measurement of  $\beta$ -spectrum shape for  $^{210}\text{Bi}$  (historically RaE) has been performed with a spectrometer based on semiconductor Si(Li) detector. This first forbidden nonunique transition has the transition form factor strongly deviated from unity, and knowledge of its spectrum would play an important role in low-background physics in the presence of  $^{210}\text{Pb}$  background. The measured transition formfactor could be approximated as  $C(W) = 1 + (-0.4470 \pm 0.0013)W + (0.0552 \pm 0.0004)W^2$ , that is in good agreement with previous studies and has significantly increased parameter precision.

DOI: [10.1103/PhysRevC.102.064329](https://doi.org/10.1103/PhysRevC.102.064329)

### I. INTRODUCTION

Precision measurements of the  $\beta$  spectra are currently very important in neutron and nuclear  $\beta$ -decay studies, as a means of searching for the effects beyond the standard model (SM) in the low energy region [1,2]. Accurate studies of nuclear  $\beta$  decays have been exploited for many years in various applications of fundamental physics problems, predominantly in neutrino physics.

In this paper we present the results of the measurement of  $^{210}\text{Bi}$   $\beta$  spectrum performed with spectrometer based on Si(Li) detectors [3,4]. The problems of  $^{210}\text{Bi}$   $\beta$  decay such as strong deviation from the allowed energy distribution, prolonged lifetime, and anomalous longitudinal electron polarization has been investigated widely starting from the 1930s in numerous experimental and theoretical works [5–18]. The situation was clarified after the assumption that the ground state of  $^{210}\text{Bi}$  is the combination of several wave functions, the calculation of nuclear matrix elements for  $\beta$  decay on the basis of the finite Fermi systems theory, and extracting the nuclear wave functions directly from the experimental data (see [19,20] and references quoted therein). The latest measurements of  $^{210}\text{Bi}$   $\beta$ -decay spectrum were performed in [20–23] via magnetic lens and solid state  $\beta$  spectrometers. The need for a precise study of  $^{210}\text{Bi}$   $\beta$  spectrum and improvement of the shape factor continues to be an important task in nuclear physics.

The bismuth isotope  $^{210}\text{Bi}$  belongs to the natural radioactive decay chain of  $^{238}\text{U}$ . As a product of the radioactive gas  $^{222}\text{Rn}$  and the subsequent long-lived  $^{210}\text{Pb}$ , the isotope  $^{210}\text{Bi}$  is present inside or on the surface of almost all structural materials. At present, the precise measurement of  $^{210}\text{Bi}$   $\beta$  spectrum remains a crucial task for background modeling of modern neutrino detectors, as well as for the dark matter searches or other low-background experiments. In particular, the shape of  $^{210}\text{Bi}$   $\beta$  spectrum is very similar to the spectrum of recoil electrons originated from scattering of solar CNO neutrinos [24], so in order to extract the Carbon-Nitrogen-

Oxygen (CNO) signal it is necessary to determine the shape of the  $\beta$  spectrum with sufficient accuracy.

### II. EXPERIMENTAL SETUP

Magnetic [25,26] and electrostatic [27,28]  $\beta$  spectrometers possess the superior energy resolution, but it comes at the cost of large scale and complexity of such experimental setup. Since the electron free path at 3 MeV of kinetic energy (which is, basically, the maximum  $\beta$ -transition energy for long-living isotopes) does not exceed  $2 \text{ g/cm}^3$ , solid state scintillation and ionization detectors were effectively employed for detection of  $\beta$  electrons [29,30]. The main drawback of the solid state scintillators is their relatively poor energy resolution, which stands at approximately 10% at 1 MeV as well as nonlinearity effects related with quenching and emission of Čerenkov radiation.

In case of semiconductor detectors, there is a significant probability of back-scattering from the detector surface that depends upon the detector material. The most widespread silicon-based semiconductors have the backscattering probability of the order of 10% for 100 keV electrons at normal incidence [31]. In case of the electron energies above 1 MeV and high  $Z$  detector materials, it also becomes important to take the bremsstrahlung into account. Still, good linearity of these detectors combined with high energy resolution gives them a lot of advantages with respect to other types of solid state detectors.

The layout of the  $\beta$  spectrometer used for our measurements was based on a simple “target-detector” geometry [3,4]. The Si(Li) detector with sensitive region diameter of 15.1 mm and thickness of 6.6 mm was produced by standard diffusion-drift technology [32]. Since the detector sensitive region did not cover the whole detector, it was fitted with a tungsten collimator (14 mm diameter) that ensured that incident electrons were either backscattered or stopped in the  $i$  region of the detector.

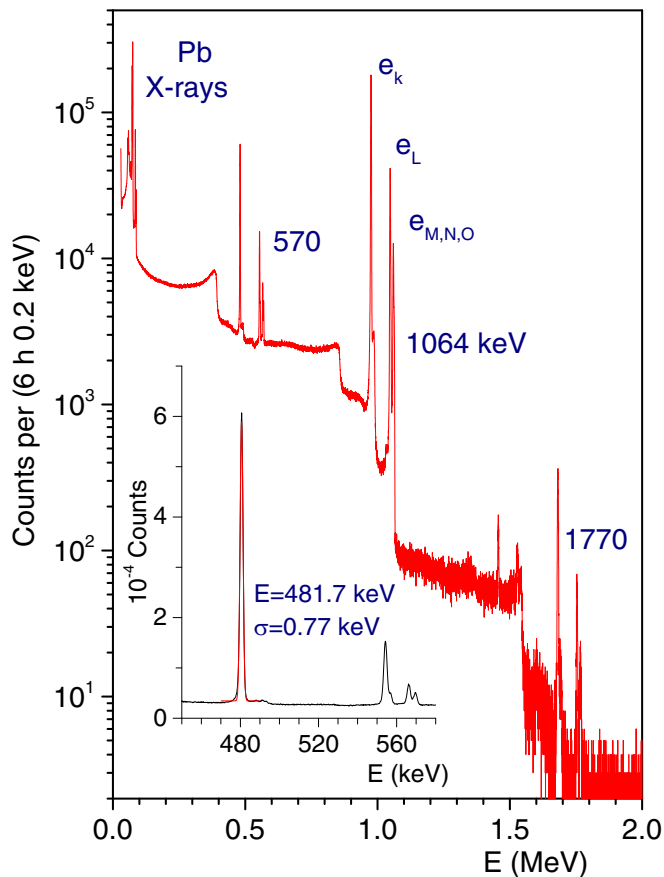


FIG. 1. The spectrum of  $^{207}\text{Bi}$  source measured with the Si(Li) detector in energy range of (0.01–2.0) MeV. The inset shows the electron peaks corresponding to internal conversion from  $K$ ,  $L$ ,  $M$ , and  $N$  shells of the 570 keV nuclear level.

The whole setup was located in a vacuum cryostat and cooled down to liquid nitrogen temperature. The setup was equipped with a moderate passive shielding (50 mm of iron and 10 mm of copper) that allowed for reduction of the environmental backgrounds by a factor of 7, down to  $2.6 \times 10^{-1}$  counts/s above 50 keV.

The detector was operated with bias voltage of 800 V. The readout was processed with a charge-sensitive preamplifier with resistive feedback and cooled field-effect transistor (FET) transistor of the first cascade. The preamplifier signal was processed with a standard CR-3RC analog shaper and digitized with a 14-bit Analog-to-Digital Converter (ADC). The energy resolution determined for 59.6 keV  $\gamma$  line of  $^{241}\text{Am}$  turned out to be  $\text{FWHM} = 900$  eV for the full width at half-maximum.

In order to determine the main characteristics of the spectrometer, we used a  $^{207}\text{Bi}$  source, providing  $\gamma$  and x rays, conversion, and Auger electrons. The  $^{207}\text{Bi}$  source with an activity of  $10^4$  Bq was placed inside the vacuum cryostat at a distance of 14 mm above the Si(Li) detector surface. The  $^{207}\text{Bi}$  spectrum, measured with the Si(Li) detector, is shown in Fig. 1 for the interval (0.01–2.0) MeV [3].

Three of the most intense  $^{207}\text{Bi}$   $\gamma$  lines had energies of 569.7 keV, 1063.7 keV, and 1770.2 keV and are emitted

with probabilities of 0.977, 0.745, and 0.069 per single  $^{207}\text{Bi}$  decay, respectively [33,34]. The corresponding peaks of the conversion electrons from  $K$ ,  $L$ , and  $M$  shells are clearly visible in the spectrum in Fig. 1. The electron energy resolution determined via 480 keV line is  $\text{FWHM} = 1.8$  keV. Energy calibration performed using Pb  $K_{\alpha 1}$  x ray and  $\gamma$  line with energies of 74.97 keV and 569.70 keV, correspondingly, predicts the position of 975.66 keV conversion electrons peak with an accuracy better than 0.3 keV.

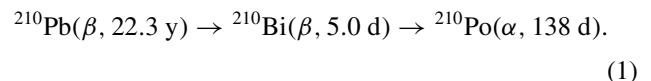
The low-energy part of the  $^{207}\text{Bi}$  spectrum was used for evaluation of the thickness of the nonsensitive layer on the surface of Si(Li) detector. This area contained a set of peaks corresponding to Pb x rays from  $K$  and  $L$  series and Auger electrons. The observed position of 56.94 keV Auger peak ( $e_{K,L_1,L_2}$ ) appeared to be at 56.22 keV. Taking the 500 Å the gold coating into account, the measured energy loss of 720 eV for 57 keV electrons corresponded to 4700 Å of the nonsensitive layer.

The planar  $^{210}\text{Bi}$  source was prepared with the method of thermal oxidation [35]. The polished stainless steel foil with diameter of 24 mm and thickness of 11  $\mu\text{m}$  was used as substrate for application of  $^{210}\text{Bi}$ . A water-alcohol  $^{210}\text{Bi}$ -containing solution was deposited onto the oxidized surface of the foil. The solution was air-dried and then annealed for 3 min at the temperature of 300°C in order to diffuse the radioactive isotope into the oxidized surface of the substrate.

This technique is capable of producing the source of negligibly small thickness, suppressing the effects caused by the attenuation and scattering of the electrons inside the bulk material of the source itself. The source produced in such a way decreases the systematic uncertainties of the measurement, since mentioned effects are usually difficult to simulate due to the complications with source geometry reconstruction.

### III. THE RESULTS OF MEASUREMENTS

The natural radioactivity of the  $^{238}\text{U}$  and  $^{232}\text{Th}$  families, along with the long-lived  $^{40}\text{K}$  isotope, are the main sources of background for neutrino physics and dark matter searches at energies below 3–5 MeV. The main decay modes and half-life  $T_{1/2}$  values of daughter nuclei produced by a long-lived  $^{210}\text{Pb}$  isotope are



The end-point energies of the  $^{210}\text{Pb}$  and  $^{210}\text{Bi}$   $\beta$  spectra are 63.5 keV and 1162 keV, respectively, while the energy of  $^{210}\text{Po}$   $\alpha$  particles is 5.304 MeV [33,34]. Since our  $^{210}\text{Pb}$  source was custom-made and intentionally purified from other lead isotopes, the equilibrium of the decay chain (1) had not yet been established at the time of measurement.

Figure 2 shows the low-energy region of the measured spectrum determined mainly by  $^{210}\text{Pb}$  decays. Transition from 46.5 keV nuclear level of  $^{210}\text{Bi}$  has significant internal conversion coefficient ( $e/\gamma \simeq 20$ , [33]). Therefore, the electron peaks corresponding to conversion from  $L$ ,  $M$ , and  $N$  shells are clearly visible in the spectrum.

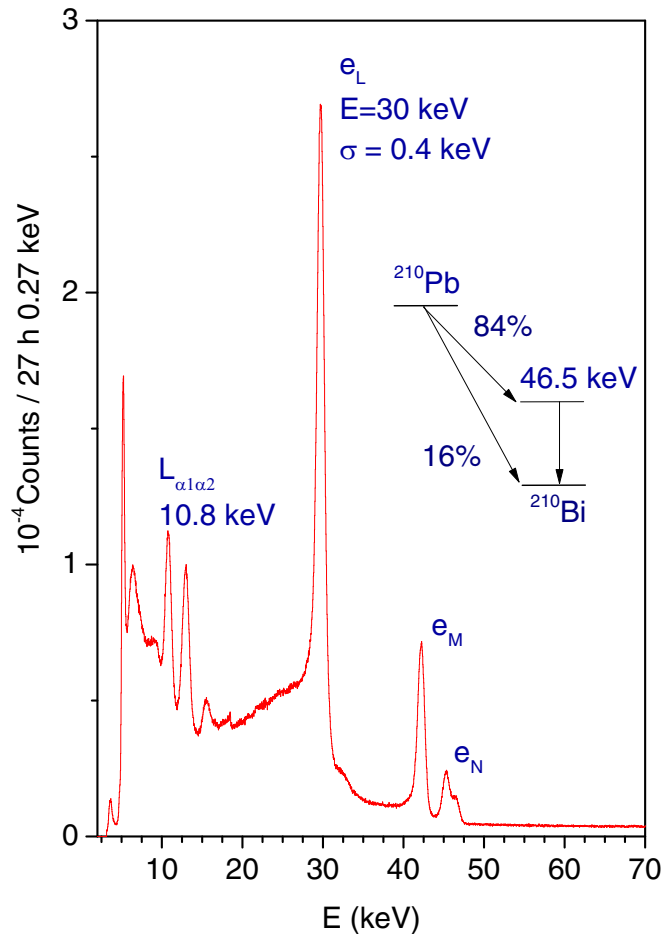


FIG. 2. Low energy part of  $^{210}\text{Pb} \rightarrow ^{210}\text{Bi}$  spectra measured with Si(Li) detector. The inset shows the decay scheme of  $^{210}\text{Pb}$ .

The energy resolution of Si(Li) detector determined for 30 keV electron conversion line was determined to be  $\text{FWHM} = 1.0$  keV and lower energy detection threshold was about 5 keV. The kinetic energy of the recoil nucleus from the  $\alpha$  decay of  $^{210}\text{Po}$  is 100 keV. The wide peak that looks like the left shoulder of  $e_L$  peak is probably associated with these events. The spectrum also shows the peaks of characteristic 10.8 keV and 13.0 keV  $L_{\alpha 1}$  and  $L_{\beta 1}$  x rays and the wider peak of 15.5 keV Auger  $e_{LNM}$  electrons.

The whole spectrum in the energy range of (0.05–5.5) MeV is shown in the Fig. 3. The energy resolution of 5407 keV  $^{210}\text{Po}$   $\alpha$  peak was determined to be  $\text{FWHM} = 26$  keV. The peak is slightly asymmetric due to the final thickness of the target and possible other  $\alpha$  impurities. The background level near the end-point energy of  $^{210}\text{Bi}$   $\beta$  spectrum amounted to 0.18 counts/h/keV and that was contributed mainly by Compton scattering of 1.46 MeV  $\gamma$  quanta of  $^{40}\text{K}$  passing through the passive shielding. The maximum energy of recoil electrons at the edge of Compton scattering is  $E_C = 2E^2/(2E + m_e) = 1243$  keV that differs significantly from the  $^{210}\text{Bi}$   $\beta$ -decay endpoint energy.

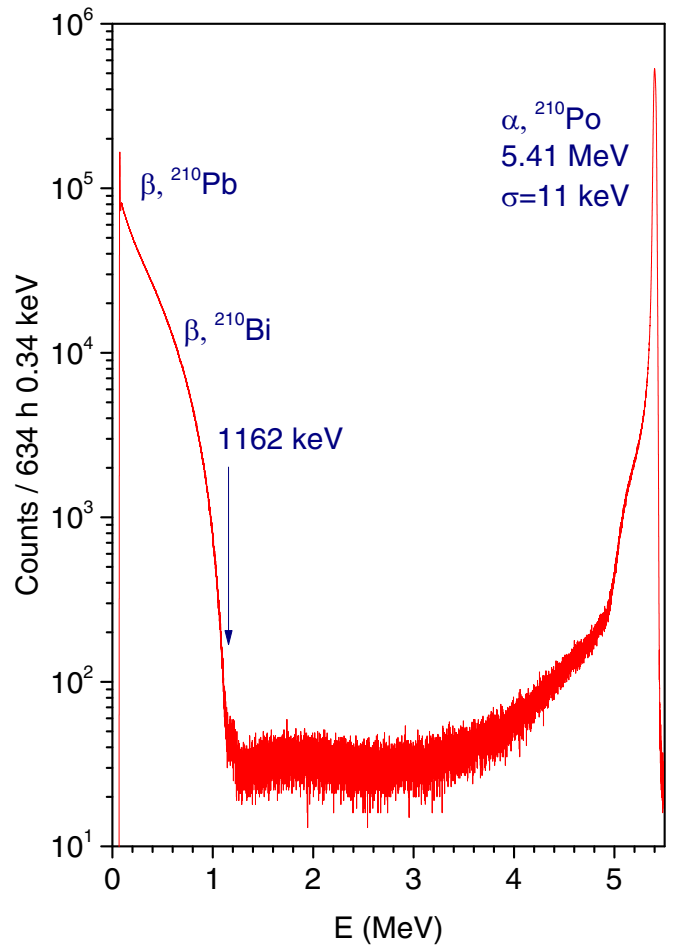


FIG. 3. The energy spectrum of  $^{210}\text{Pb} \rightarrow ^{210}\text{Bi} \rightarrow ^{210}\text{Po}$  source measured with the Si(Li) detector in energy range of (0.05–5.5) MeV. The  $\beta$  spectrum of  $^{210}\text{Bi}$  has 1162 keV end-point energy, the  $\alpha$  decay of  $^{210}\text{Po}$  leads to 5.4 MeV peak.

The counting rate in the range from 80 keV to 1.5 MeV was  $27 \text{ s}^{-1}$ , that with  $1 \mu\text{s}$  pile-up rejection time leads to negligible pile-up spectrum and dead time of the spectrometer.

The data were obtained during 634 hours of data taking in short 1-h series used for stability control. To determine the energy calibration  $E = a + bN$  [where  $E$  is a Si(Li) visible energy and  $N$  is an ADC channel number], the position of 46.5 keV  $\gamma$  peak and the value of  $^{210}\text{Bi}$  end-point energy  $E_0 = 1162$  keV measured with high accuracy in other experiments [33,34] were used.

During the fitting of the spectrum, the calibration slope  $b$  equal to the analyzer channel width was free, while the value of the parameter  $a$  was fixed by 46.5 keV peak position. The differences of fitting parameters for the all 1-h runs are in agreement with their statistical uncertainties. The fact that equilibrium in Eq. (1) was not achieved could not affect the fitting results for different series, if only because the contribution of the tail of  $\alpha$  particles to the  $\beta$ -spectrum region was very small. The total number of registered  $^{210}\text{Bi}$  decays was  $1.0 \times 10^8$ .

#### IV. DATA ANALYSIS

The energy distribution  $S(W)$  of  $\beta$ -particles emitted in  $\beta$ -decay process could be expressed as

$$S(W) = PW(W - W_0)^2 \times F(W, Z) \times C(W), \quad (2)$$

where  $P$  and  $T$  are the electron momentum and energy,  $W = T/mc^2 + 1$  is full electron energy,  $W_0 = T_0/mc^2 + 1$  is  $\beta$ -spectrum end-point energy,  $F(W, Z)$  is the electron Fermi function that takes into account electromagnetic interaction of the outgoing electron with the atom and  $C(W)$  is the transition nuclear form factor that considers the effects of internal nuclear interactions.

The Fermi function  $F(W, Z)$  is historically derived in approximation of a point-like nuclei without consideration of the atomic shells [36] that means that comparison with experiments using this model needs application of the same approximation, while the  $\beta$  spectrum for practical applications would need a more profound calculation of the Fermi function that was performed according to [37–39].

The transition investigated in this work is of forbidden type and the nuclear form-factor  $C(W)$  is expected to deviate from unity and is the main subject of the measurement. Since the shape factor of first forbidden nonunique transition with such parity-momentum relations can be expressed with sufficient accuracy by a second degree polynomial, we choose the  $C(W)$  parametrization as in [20]

$$C(W) = 1 + C_1W + C_2W^2 \quad (3)$$

with generic values of parameters  $C_1$  and  $C_2$  that were defined through maximum likelihood fit with  $\chi^2$  likelihood function.

The final model of the experimental spectrum expresses as

$$N(E) = \int_{E/mc^2+1}^{W_0} S(W) \times R(W, E) dW, \quad (4)$$

where  $R(W, E)$  is the spectrometer normalized response function obtained with Monte Carlo simulation of electrons with energy  $W$  exiting the source with uniform distribution within the source and uniform distribution of their momenta directions.

Since the setup in use has the classical “target-detector” geometry, it is quite important to take into account the detector response function that would contain a long low-energy tail caused by fraction of electrons backscattered from the detector as well as by bremsstrahlung exit from the detector crystal. The Si(Li) detector has  $i$ -region thickness exceeding the stopping range of an electron with endpoint energy of 1162 keV and thus the geometry of irradiated regions of the setup is quite well established. This allows to account for the detector energy response through a precise simulation with the Monte Carlo method. We used GEANT4.10.04 simulation package [40] with the standard G4EmStandardPhysics\_option4 package of electromagnetic interactions.

The package choice was mainly motivated by the single scattering model for electrons, that is the most promising among standard ones according to [41,42]. The simulation was including modeling of the detector entrance windows, collimator and holders according to the physical setup geometry.

As the response function model is based on the simplified interaction models used in the simulation, it is important to estimate the uncertainties concerning its imperfection. Consideration of these uncertainties was performed through analytical modification of the response function as

$$\tilde{R}(E, W) = \begin{cases} R(E, W) \times (1 + A \ln(BW)) & \text{if } E < T - 5\sigma \\ R(E, W) & \text{if } E > T - 5\sigma \end{cases}, \quad (5)$$

where  $\sigma$  is the detector resolution at kinetic energy  $T$  and  $A, B$  are free parameters. Eventually, six parameters were free in the fit: the common normalization coefficient, the slope of the energy calibration, the form factor parameters  $C_1$  and  $C_2$ , and response function parameters  $A$  and  $B$ .

The dependence  $A \ln(BW)$  used for the variation of the response function tail approximately corresponds to the uncertainties of the response function for different GEANT4 simulation packages [41]. The response function was renormalized to conserve detection efficiency of the original simulation.

The fit range has the lower bound that comes from presence of  $^{210}\text{Pb}$  in the source that covers the low-energy region. Considering that the nuclear form-factor  $C(W)$  depends only upon momenta of the electron and neutrino one should not expect sudden behavior in the lower tenth of the energy spectrum so this lower bound should not be important for the form-factor establishment.

The fit with canonical Fermi function  $F_0(W, Z)$  was performed in the energy range 120–1175 keV with flat background approximation. The Fermi function was calculate according to [36] as

$$F_0(W, Z) = 4(2pR(A))^{2(\gamma-1)} e^{(\pi Y)} \frac{|\Gamma(\gamma + iY)|}{\Gamma^2(1 + 2\gamma)}, \quad (6)$$

where  $Y = \alpha ZW/p$  and  $\gamma = \sqrt{1 - \alpha^2 Z^2}$ ,  $\alpha$  is the fine-structure constant and  $R$  is the nuclear radius defined as  $R = 0.0029 \times A^{1/3} + 0.0063 \times A^{2/3} - 0.017 \times A^{-1}$ .

The fit results are shown in Fig. 4. The obtained minimum of  $\chi^2/\text{NDF} = 1775.3/1705$  corresponds to Pearson  $P$  value = 0.12 and form-factor parameters  $C_1 = -0.4523 \pm 0.0031$  and  $C_2 = 0.0560 \pm 0.0008$ . The easily computed values of  $F_0(W, Z)$  Eq. (6) together with obtained coefficients  $C_1$  and  $C_2$  allows to calculate the shape of the  $\beta$  spectrum that references to our measurements.

In order to have a fair comparison with the results of [20,22] we performed the fit with the Fermi function  $F(W, Z)$  calculated in accordance with formalism presented in [37], attempting to improve the precision of the analytical description. In this work  $F(E, Z)$  was enhanced by including second and third terms of  $pr$ -power expansion of electron wave function at small values of  $r$  [ $F_0(E, Z)$  is obtained by neglecting all but the first term]. Also, additional corrections were included, taking the finite size of the nucleus and atomic shell screening into account [43,44]. The values of  $F(E, Z) = F_0(E, Z)\chi\eta$  used in the calculation were taken from Table 14 of [37] for  $Z = 83$  and  $A = 210$ .

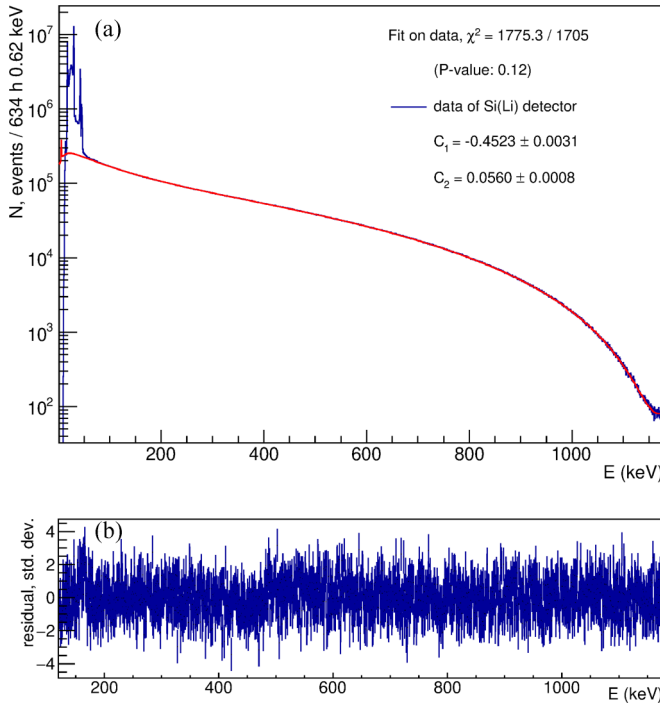


FIG. 4. Experimental spectrum fit with parabolic form-factor  $C(W)$  and Fermi function  $F_0(W, Z)$ , computed in approximation of a point-like nucleus [37]. The  $\chi^2$  fit was performed in the energy range 120–1175 keV with flat background approximation.

The fit range was increased with respect to the improved  $F(W, Z)$  that takes into account the nucleus final size and the screening corrections. The same procedure gives the form-factor parameters as  $C_1 = -0.4339 \pm 0.0012$  and  $C_2 = 0.0513 \pm 0.0004$ . One can compare these values with  $C'_1 = -0.46 \pm 0.01$  and  $C'_2 = 0.0586 \pm 0.002$  obtained in [20]. The errors of  $C_1$ ,  $C_2$  obtained in the present work are more than five times less, however, the parameters  $C_1$ ,  $C_2$  and  $C'_1$ ,  $C'_2$  are consistent with each other within the  $1.5 \sigma$ .

The final fitting procedure was repeated using the classic definition of the Fermi function with several corrections that included atomic shell screening effect [45], finite size distribution of electromagnetic and weak charge inside nucleus [46], and quantum electrodynamics (QED) radiative corrections [39,47]. The final  $F(E, Z)$  had the following form:

$$F(E, Z) = F_0(E, Z) \times S(E, Z) \times L_0(E, Z) \times M(E, Z) \times G_\beta(E), \quad (7)$$

where  $E$  is full electron energy,  $Z$  is the charge of a daughter nucleus,  $F_0(E, Z)$  is Fermi function,  $S(E, Z)$  screening correction,  $L_0(E, Z)$  and  $M(E, Z)$  are electromagnetic and weak finite size corrections, and  $G_\beta(E)$  is radiative correction. The results of the final fitting procedure are given in Fig. 5.

Implication of a more precise Fermi function allowed to lower energy threshold down to 100 keV, providing good  $P$  value = 0.12 that is an evidence of better agreement of the corrected  $\beta$  spectrum with the experimental data.

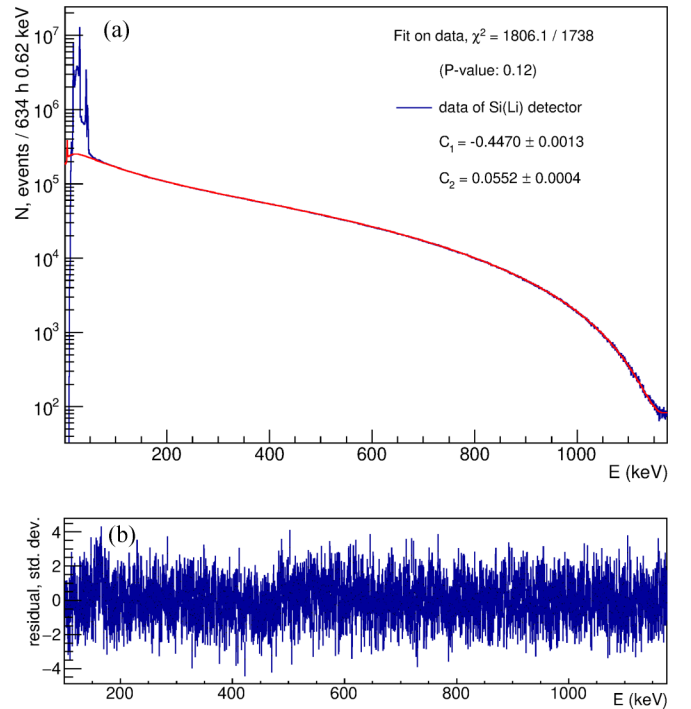


FIG. 5. Experimental spectrum fit with parabolic form-factor  $C(W)$  and Fermi function  $F(W, Z)$ , computed according to [38,45]. The  $\chi^2$  fit was performed in the energy range 100–1175 keV with flat background approximation.

The minimum of  $\chi^2/\text{NDF} = 1806.1/1738$  corresponds to form-factor parameters  $C_1 = -0.4470 \pm 0.0013$  and  $C_2 = 0.0552 \pm 0.0004$ . These values  $C_1$  and  $C_2$  are obtained taking into account the most complete knowledge of the interactions emitted electron with atom. One should note that the parameters  $C_1$  and  $C_2$  have quite strong correlation in the fit of the experimental data, having the correlation coefficients of 0.987 (Fig. 4) and 0.96 (Fig. 5). The inclusion of the quadratic term in the energy calibration and an additional pull term in the fitting procedure leads to an increase of  $C_1$  and  $C_2$  errors by less than 5% without changing the central values.

The fits performed have shown convergence of parameter  $A$  to null, showing that with the current experimental statistics the Monte Carlo simulation of the spectrometer response gives results consistent with the data. The conservative approach demonstrates the fact that inclusion of parameters  $A$  and  $B$  in the fit leads to increase errors of  $C_1$  and  $C_2$  by approximately a factor of three.

The present results are compared with obtained in works [22] [Daniel (1962)] and [20] [Carles & Malonda (1996)] in Fig. 6. The upper part of the figure shows the electron spectra. To determine the Daniel (1962) spectrum, we used the data from Table 2 [22] and the Fermi function from [37]. The Carles and Malonda (1996) spectrum was calculated in accordance with the parameters  $C_1$  and  $C_2$  given in [20]. The figure shows two electron spectra obtained in the present work for  $F_0(W, Z)$  and  $F(W, Z)$  Fermi functions according to [36] and [38,45]. All  $\beta$  spectra were normalized to unity.

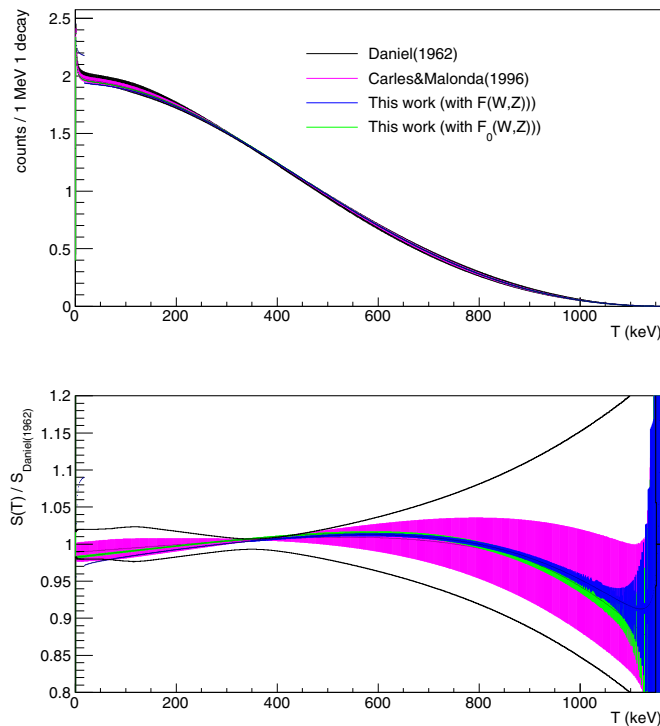


FIG. 6. Comparison of the spectra measured by Daniel (1962) [22] and Carles & Malonda (1996) [20] with the present study (top). Ratio to Daniel (1962) spectrum (bottom). Daniel (1962) spectrum errors are shown by solid black lines.

Figure 6 shows also the ratio of Carles and Malonda (1996) and present work spectra to Daniel (1962) spectrum [22]. Daniel (1962) spectrum errors determined by fit are shown by solid black lines.

Because  $C_1$  and  $C_2$  have quite strong correlation, in order to estimate uncertainties on the form factor curve shown at Fig. 6

we applied the Monte Carlo method sampling the form-factor parameters according to two-dimensional Gaussian distribution that includes the correlation coefficient obtained in the fit. One can see that both of our spectra are consistent with Daniel (1962) and Carles & Malonda (1996) spectra within uncertainties. The current study shows significantly increased precision with respect to the previous studies.

## V. CONCLUSIONS

The spectrometer based on the Si(Li) detector was used to precisely measure the  $\beta$  spectrum of  $^{210}\text{Bi}$  nuclei. As a result of the 634 h measurements with a total number of  $1.0 \times 10^8$  of registered electrons it was established that the  $\beta$  spectrum is described by form-factor  $C(W) = 1 + (-0.4523 \pm 0.0031)W + (0.0560 \pm 0.0008)W^2$  if the Fermi function is calculated according to formula (6) for a point-like nucleus. The obtained values of the parameters  $C_1$  and  $C_2$  together with Eq. (6) can be used for calculation of the electron spectrum of  $^{210}\text{Bi}$ .

When the additional above-mentioned corrections to the Fermi function are taken into account, the form-factor parameters are equal to  $C_1 = (-0.4470 \pm 0.0013)$  and  $C_2 = (0.0552 \pm 0.0004)$ , that can be useful for the calculation of specific nuclear matrix elements. The obtained parameters of the form-factor are in agreement with the previous studies and have significantly increased precision.

## ACKNOWLEDGMENTS

This work was supported by the Russian Foundation for Basic Research (Projects No. 19-02-00097 and No. 20-02-00571).

- [1] P. Herczeg, Beta decay beyond the standard model, *Prog. Part. Nucl. Phys.* **46**, 413 (2001).
- [2] J. S. Nico and W. Michael Snow, Fundamental neutron physics, *Annu. Rev. Nucl. Part. Sci.* **55**, 27 (2005).
- [3] I. E. Alexeev, S. V. Bakhlanov, N. V. Bazlov, E. A. Chmel, A. V. Derbin, I. S. Drachnev, I. M. Kotina, V. N. Muratova, N. V. Pilipenko, D. A. Semyonov, E. V. Unzhakov, and V. K. Yeremin, Beta-spectrometer with Si-detectors for the study of  $^{144}\text{Ce} - ^{144}\text{Pr}$  decays, *Nucl. Instrum. Methods Phys. Res. A* **890**, 64 (2018).
- [4] N. V. Bazlov, S. V. Bakhlanov, A. V. Derbin, I. S. Drachnev, V. K. Eremin, I. M. Kotina, V. N. Muratova, N. V. Pilipenko, D. A. Semyonov, E. V. Unzhakov, and E. A. Chmel, A beta spectrometer based on silicon detectors, *Instrum. Exp. Tech.* **61**, 323 (2018).
- [5] J. S. O'Conor, The beta-ray spectrum of Radium E, *Phys. Rev.* **52**, 303 (1937).
- [6] L. Harold Martin and A. Alan Townsend, The  $\beta$ -ray spectrum of Ra E, *Proc. R. Soc. Lond. A* **170**, 190 (1939).
- [7] G. J. Neary and J. D. Cockcroft, The beta-ray spectrum of Radium E, *Proc. R. Soc. London A* **175**, 71 (1940).
- [8] E. J. Konopinski and G. E. Uhlenbeck, On the Fermi theory of  $\beta$ -radioactivity. II. The "forbidden" spectra, *Phys. Rev.* **60**, 308 (1941).
- [9] N. Newby and E. J. Konopinski, Nuclear states in the RaE  $\beta$ -decay, *Phys. Rev.* **115**, 434 (1959).
- [10] J.-I. Fujita, Conserved current hypothesis and the beta decay of RaE, *Phys. Rev.* **126**, 202 (1962).
- [11] Y. E. Kim and J. O. Rasmussen, Energy levels of  $\text{Bi}^{210}$  and  $\text{Po}^{210}$  and the shell-model residual force, *Nucl. Phys.* **47**, 184 (1963).
- [12] R. M. Spector, Shell model investigation of RaE beta-decay, *Nucl. Phys.* **40**, 338 (1963).
- [13] J. Sodemann and A. Winther, Nuclear matrix elements for the  $\beta$ -decay of  $\text{Bi}^{210}(\text{RaE})$ , *Nucl. Phys.* **69**, 369 (1965).
- [14] J. Damgaard, R. Broglia, and C. Riedel, First-forbidden  $\beta$ -decays in the lead region, *Nucl. Phys. A* **135**, 310 (1969).
- [15] S. A. Fayans and V. A. Khodel, Calculations of nuclear matrix elements for beta-decay of RaE, *Phys. Lett. B* **31**, 99 (1970).
- [16] H. Rebel, R. Lohken, and G. Schatz, A numerical method of analyzing beta decay measurements and its application to the

- $1^- \rightarrow 0^+$  transitions of  $^{170}\text{Tm}$ ,  $^{186}\text{Re}$  and  $^{210}\text{Bi}$ , *Z. Phys. A* **245**, 425 (1971).
- [17] M. Morita, M. Yamada, J.-I. Fujita, A. Fujii, H. Ohtsubo, R. Morita, K. Ikeda, Y. Yokoo, M. Hiro-Oka, and K. Takahashi, Nuclear structure studied from weak and related processes, *Prog. Theor. Phys. Suppl.* **48**, 41 (1971).
- [18] K. Ebert, W. Wild, and F. Krmpotić, A nuclear structure study of the  $\beta$ -decay of  $^{210}\text{Bi}(\text{RaE})$ , *Phys. Lett. B* **58**, 132 (1975).
- [19] H. Behrens and L. Szybisz, On the  $\beta$ -decay  $^{210}\text{Bi}(\text{RaE}) \rightarrow ^{210}\text{Po}(\text{RaF})$ , *Nucl. Phys. A* **223**, 268 (1974).
- [20] A. Grau Carles and A. Grau Malonda, Precision measurement of the RaE shape factor, *Nucl. Phys. A* **596**, 83 (1996).
- [21] E. A. Plassmann and L. M. Langer, Beta spectrum of Radium E, *Phys. Rev.* **96**, 1593 (1954).
- [22] H. Daniel, Das  $\beta$ -spektrum des RaE, *Nucl. Phys.* **31**, 293 (1962).
- [23] D. Flothmann, W. Wiesner, R. Löhken, and H. Rebel,  $\beta$ -Spektroskopie mit Halbleiterdetektoren beim Zerfall von  $^{32}\text{P}$ ,  $^{49}\text{Sc}$ ,  $^{204}\text{Tl}$  und  $^{210}\text{Bi}$ , *Z. Phys. A* **225**, 164 (1969).
- [24] M. Agostini, K. Altenmüller, S. Appel, V. Atroshchenko, Z. Bagdasarian, D. Basilico, G. Bellini, J. Benziger, G. Bonfini, D. Bravo, B. Caccianiga, F. Calaprice, A. Caminata, L. Cappelli, S. Caprioli, M. Carlini, P. Cavalcante, F. Cavanna, A. Chepurnov, K. Choi, L. Collica, D. D'Angelo, S. Davini, A. Derbin, X. F. Ding, A. Di Ludovico, L. Di Noto, I. Drachnev, K. Fomenko, A. Formozov, D. Franco, F. Gabriele, C. Galbiati, M. Gschwender, C. Ghiano, M. Giammarchi, A. Goretti, M. Gromov, D. Guffanti, T. Houdy, E. Hungerford, Aldo Ianni, Andrea Ianni, A. Jany, D. Jeschke, S. Kumaran, V. Kobychov, G. Korga, T. Lachenmaier, M. Laubenstein, E. Litvinovich, P. Lombardi, L. Ludhova, G. Lukyanchenko, L. Lukyanchenko, I. Machulin, G. Manuzio, S. Marocci, J. Maricic, J. Martyn, E. Meroni, M. Meyer, L. Miramonti, M. Misiaszek, V. Muratova, B. Neumair, M. Nieslony, L. Oberauer, V. Orekhov, F. Ortica, M. Pallavicini, L. Papp, Ö. Penek, L. Pietrofaccia, N. Pilipenko, A. Pocar, A. Porcelli, G. Raikov, G. Ranucci, A. Razeto, A. Re, M. Redchuk, A. Romani, N. Rossi, S. Rottenanger, S. Schönert, D. Semenov, M. Skorokhvatov, O. Smirnov, A. Sotnikov, L. F. F. Stokes, Y. Suvorov, R. Tartaglia, G. Testera, J. Thurn, E. Unzhakov, F. Villante, A. Vishneva, R. B. Vogelaar, F. von Feilitzsch, S. Weinz, M. Wojcik, M. Wurm, O. Zaimidoroga, S. Zavatarelli, K. Zuber, and G. Zuzel, Simultaneous precision spectroscopy of  $pp$ ,  $^7\text{Be}$ , and  $pep$  solar neutrinos with Borexino phase-II, *Phys. Rev. D* **100**, 082004 (2019).
- [25] K.-E. Bergkvist, A high-luminosity, high-resolution study of the end-point behavior of the tritium  $\beta$ -spectrum (I). Basic experimental procedure and analysis with regard to neutrino mass and neutrino degeneracy, *Nucl. Phys. B* **39**, 317 (1972).
- [26] E. F. Tretyakov, The high resolution toroidal beta spectrometer, *Bull. Russ. Acad. Sci. Phys.* **39**, 583 (1975).
- [27] V. M. Lobashev and P. E. Spivak, A method for measuring the electron antineutrino rest mass, *Nucl. Instrum. Methods Phys. Res. A* **240**, 305 (1985).
- [28] M. Aker, K. Altenmüller, M. Arenz, M. Babutzka, J. Barrett, S. Bauer, M. Beck, A. Beglarian, J. Behrens, T. Bergmann, U. Besserer, K. Blaum, F. Block, S. Bobien, K. Bokeloh, J. Bonn, B. Bornschein, L. Bornschein, H. Bouquet, T. Brunst, T. S. Caldwell, L. La Cascio, S. Chilingaryan, W. Choi, T. J. Corona, K. Debowski, M. Deffert, M. Descher, P. J. Doe, O. Dragoun, G. Drexlin, J. A. Dunmore, S. Dyba, F. Edzards, L. Eisenblätter, K. Eitel, E. Ellinger, R. Engel, S. Enomoto, M. Erhard, D. Eversheim, M. Fedkevych, A. Felden, S. Fischer, B. Flatt, J. A. Formaggio, F. M. Fränkle, G. B. Franklin, H. Frankrone, F. Friedel, D. Fuchs, A. Fulst, D. Furse, K. Gauda, H. Gemmeke, W. Gil, F. Glück, S. Görhardt, S. Groh, S. Grohmann, R. Grössle, R. Gumbsheimer, M. Ha Minh, M. Hackenjos, V. Hannen, F. Harms, J. Hartmann, N. Haußmann, F. Heizmann, K. Helbing, S. Hickford, D. Hilk, B. Hillen, D. Hillesheimer, D. Hinz, T. Höhn, B. Holzapfel, S. Holzmann, T. Houdy, M. A. Howe, A. Huber, T. M. James, A. Jansen, A. Kaboth, C. Karl, O. Kazachenko, J. Kellerer, N. Kernert, L. Kippenbrock, M. Kleesiek, M. Klein, C. Köhler, L. Köllenberger, A. Kopmann, M. Korzeczek, A. Kosmider, A. Kovalik, B. Krasch, M. Kraus, H. Krause, L. Kuckert, B. Kuffner, N. Kunka, T. Lasserre, T. L. Le, O. Lebeda, M. Leber, B. Lehnert, J. Letnev, F. Leven, S. Lichter, V. M. Lobashev, A. Lokhov, M. Machatschek, E. Malcherek, K. Müller, M. Mark, A. Marsteller, E. L. Martin, C. Melzer, A. Menshikov, S. Mertens, L. I. Minter, S. Mirz, B. Monreal, P. I. Morales Guzmán, K. Müller, U. Naumann, W. Ndeke, H. Neumann, S. Niemes, M. Noe, N. S. Oblath, H.-W. Ortjohann, A. Osipowicz, B. Ostrick, E. Otten, D. S. Parno, D. G. Phillips, P. Plischke, A. Pollithy, A. W. P. Poon, J. Pouryamout, M. Prall, F. Priester, M. Röllig, C. Röttele, P. C.-O. Ranitzsch, O. Rest, R. Rinderspacher, R. G. H. Robertson, C. Rodenbeck, P. Rohr, Ch. Roll, S. Rupp, M. Ryšavý, R. Sack, A. Saenz, P. Schäfer, L. Schimpf, K. Schlösser, M. Schlösser, L. Schlüter, H. Schön, K. Schönung, M. Schrank, B. Schulz, J. Schwarz, H. Seitz-Moskaliuk, W. Seller, V. Sibille, D. Siegmann, A. Skasyrskaya, M. Slezák, A. Špalek, F. Spanier, M. Steidl, N. Steinbrink, M. Sturm, M. Suesser, M. Sun, D. Tcherniakhovski, H. H. Telle, T. Thümmel, L. A. Thorne, N. Titov, I. Tkachev, N. Trost, K. Urban, D. Vénos, K. Valerius, B. A. VanDevender, R. Vianden, A. P. Vizcaya Hernández, B. L. Wall, S. Wüstling, M. Weber, C. Weinheimer, C. Weiss, S. Welte, J. Wendel, K. J. Wierman, J. F. Wilkerson, J. Wolf, W. Xu, Y.-R. Yen, M. Zacher, S. Zadorozhny, M. Zbořil, and G. Zeller, Improved Upper Limit on the Neutrino Mass from a Direct Kinematic Method by Katrin, *Phys. Rev. Lett.* **123**, 221802 (2019).
- [29] J. J. Simpson, Evidence of Heavy-Neutrino Emission in Beta Decay, *Phys. Rev. Lett.* **54**, 1891 (1985).
- [30] A. V. Derbin, A. I. Egorov, V. N. Muratova *et al.*, Search for 17-keV neutrinos in  $^{63}\text{Ni}$  beta-decay, *JETP Lett.* **58**, 1 (1993).
- [31] A. V. Derbin, A. I. Egorov, S. V. Bakhlanov *et al.*, Measurement of the  $^{45}\text{Ca}$   $\beta$ -spectrum in search of deviations from the theoretical shape, *JETP Lett.* **66**, 88 (1997).
- [32] N. V. Bazlov, A. V. Derbin, I. S. Drachnev, G. E. Gicharevich, I. M. Kotina, O. I. Konkov, N. V. Pilipenko, E. A. Chmel, S. N. Abolmasov, E. I. Terukov, and E. V. Unzhakov, Si(li) detector with ultra-thin entrance window on the diffusive lithium side, *J. Phys.: Conf. Ser.* **1400**, 055056 (2019).
- [33] E. Browne and V. S. Shirley, *Table of Isotopes* (Wiley, New York, 1978).
- [34] S. Y. F. Chu, L. P. Ekström, and R. B. Firestone, The Lund/LBNL Nuclear Data Search, 1999, <http://nucleardata.nuclear.lu.se/toi/>, Version 2.0, February 1999.
- [35] I. Alekseev and T. Kuzmina, Determination of  $^{241}\text{Pu}$  by the method of disturbed radioactive equilibrium using  $2\pi\alpha$ -counting and precision gamma-spectrometry, *Appl. Radiat. Isot.* **110**, 212 (2016).

- [36] E. Fermi, An attempt of a theory of beta radiation. I, *Z. Phys.* **88**, 161 (1934).
- [37] B. S. Dzhelepov and L. N. Zyrianova, The influence of the atomic electric field on beta-decay, USSR Acad. Sci, Leningrad, 1956.
- [38] P. Huber, Determination of antineutrino spectra from nuclear reactors, *Phys. Rev. C* **84**, 024617 (2011).
- [39] L. Hayen, N. Severijns, K. Bodek, D. Rozpedzik, and X. Mougeot, High precision analytical description of the allowed  $\beta$  spectrum shape, *Rev. Mod. Phys.* **90**, 015008 (2018).
- [40] S. Agostinelli *et al.*, GEANT4: A Simulation toolkit, *Nucl. Instrum. Methods Phys. Res. A* **506**, 250 (2003).
- [41] T. Basaglia, M. C. Han, G. Hoff, C. H. Kim, S. H. Kim, M. G. Pia, and P. Saracco, Quantitative test of the evolution of GEANT4 electron backscattering simulation, *IEEE Trans. Nucl. Sci.* **63**, 2849 (2016).
- [42] P. Dondero, A. Mantero, V. Ivanchenko, S. Lotti, T. Mineo, and V. Fioretti, Electron backscattering simulation in GEANT4, *Nuclear Instrum. Methods Phys. Res. B* **425**, 18 (2018).
- [43] L. A. Sliv, On theory of forbidden beta-transitions, *JETP* **17**, 1049 (1947).
- [44] M. E. Rose, A note on the possible effect of screening in the theory of beta-disintegration, *Phys. Rev.* **49**, 727 (1936).
- [45] W. Buhring, The screening correction to the Fermi function of nuclear  $\beta$ -decay and its model dependence, *Nucl. Phys. A* **430**, 1 (1984).
- [46] D. H. Wilkinson, Evaluation of beta-decay: II. Finite mass and size effects, *Nucl. Instrum. Methods Phys. Res. A* **290**, 509 (1990).
- [47] A. Sirlin, General properties of the electromagnetic corrections to the beta decay of a physical nucleon, *Phys. Rev.* **164**, 1767 (1967).